

# Effect of the Energy of Consciousness (The Trivedi Effect<sup>®</sup>) on Physicochemical, Thermal, Structural, and Behavioral Properties of Magnesium Gluconate

Mahendra Kumar Trivedi<sup>1</sup>, Alice Branton<sup>1</sup>, Dahryn Trivedi<sup>1</sup>, Gopal Nayak<sup>1</sup>, Michael Peter Ellis<sup>1</sup>, James Jeffery Peoples<sup>1</sup>, James Joseph Meuer<sup>1</sup>, Johanne Dodon<sup>1</sup>, John Lawrence Griffin<sup>1</sup>, John Suzuki<sup>1</sup>, Joseph Michael Foty<sup>1</sup>, Judy Weber<sup>1</sup>, Julia Grace McCammon<sup>1</sup>, Karen Brynes Allen<sup>1</sup>, Kathryn Regina Sweas<sup>1</sup>, Lezley Jo-Anne Wright<sup>1</sup>, Lisa A. Knoll<sup>1</sup>, Madeline E. Michaels<sup>1</sup>, Margaret Kweya Wahl<sup>1</sup>, Mark E. Stutheit<sup>1</sup>, Michelle Barnard<sup>1</sup>, Muriel Mae Ranger<sup>1</sup>, Paromvong Sinbandhit<sup>1</sup>, V. J. Kris Elig<sup>1</sup>, Kalyan Kumar Sethi<sup>2</sup>, Parthasarathi Panda<sup>2</sup>, Snehasis Jana<sup>2,\*</sup>

<sup>1</sup>Trivedi Global, Inc., Henderson, Nevada, USA

<sup>2</sup>Trivedi Science Research Laboratory Pvt. Ltd., Bhopal, Madhya Pradesh, India

## Email address:

publication@trivedieffect.com (S. Jana)

\*Corresponding author

## To cite this article:

Mahendra Kumar Trivedi, Alice Branton, Dahryn Trivedi, Gopal Nayak, Michael Peter Ellis, James Jeffery Peoples, James Joseph Meuer, Johanne Dodon, John Lawrence Griffin, John Suzuki, Joseph Michael Foty, Judy Weber, Julia Grace McCammon, Karen Brynes Allen, Kathryn Regina Sweas, Lezley Jo-Anne Wright, Lisa A. Knoll, Madeline E. Michaels, Margaret Kweya Wahl, Mark E. Stutheit, Michelle Barnard, Muriel Mae Ranger, Paromvong Sinbandhit, V. J. Kris Elig, Kalyan Kumar Sethi, Parthasarathi Panda, Snehasis Jana. Effect of the Energy of Consciousness (The Trivedi Effect<sup>®</sup>) on Physicochemical, Thermal, Structural, and Behavioral Properties of Magnesium Gluconate. *Chemical and Biomolecular Engineering*. Vol. 2, No. 2, 2017, pp. 113-123. doi: 10.11648/j.cbe.20170202.16

**Received:** February 7, 2017; **Accepted:** February 18, 2017; **Published:** March 6, 2017

---

**Abstract:** Magnesium gluconate is an organometallic pharmaceutical compound used for the prevention and treatment of hypomagnesemia. The objective of the current research work was to examine the influence of The Trivedi Effect<sup>®</sup>-Energy of Consciousness Healing Treatment (Biofield Energy Treatment) on magnesium gluconate for the alteration in the physicochemical, structural, thermal and behavioral properties using PXRD, PSD, FT-IR, UV-vis spectroscopy, TGA, and DSC analysis. Magnesium gluconate was divided into two parts – one part was control without any Biofield Energy Treatment, while another part was treated with The Trivedi Effect<sup>®</sup>-Energy of Consciousness Healing Treatment remotely by twenty renowned Biofield Energy Healers and defined as The Trivedi Effect<sup>®</sup> treated sample. The PXRD analysis exhibited that the crystallite size of the treated sample was remarkably altered from -63.63% to 80.14% compared with the control sample. The average crystallite size was significantly reduced by 22.14% in the treated sample compared with the control sample. The particle size values in the treated sample at  $d_{10}$  and  $d_{50}$  values were significantly decreased by 4.41% and 8.67% respectively, whereas at  $d_{90}$  value was increased by 3.99% compared to the control sample. The surface area analysis revealed that surface area of the treated sample was significantly increased by 5.21% compared with the control sample. The FT-IR and UV-vis analysis showed that structure of the magnesium gluconate remained identical in both the treated and control samples. The TGA analysis shown four steps thermal degradation of both the samples and the total weight loss of the treated sample was significantly decreased by 4.29% compared with the control sample. The melting temperature of the control and treated samples were 171.02°C and 170.93°C, respectively. The latent heat of fusion was significantly increased by 32.33% in the treated sample compared with the control sample. The TGA and DSC analysis indicated that the thermal stability of the treated sample was significantly improved compared with the control sample. The current study revealed that The Trivedi Effect<sup>®</sup>-Energy of Consciousness Healing Treatment might produce a new polymorphic form of magnesium gluconate, which could be more soluble and bioavailable along with improved thermal stability compared with the untreated compound. The treated sample could be more stable during manufacturing, delivery or storage conditions than the untreated sample. Hence, The Trivedi Effect<sup>®</sup> Treated magnesium gluconate would be very useful to design better nutraceutical/pharmaceutical formulations

that might offer better therapeutic responses against inflammatory diseases, immunological disorders, stress, aging, and other chronic infections.

**Keywords:** Biofield Energy Healing Treatment, Consciousness Energy Healers, The Trivedi Effect<sup>®</sup>, Magnesium Gluconate, PXRD, Particle Size, Surface Area, TGA, DSC

---

## 1. Introduction

Magnesium gluconate is a divalent organometallic nutraceutical/pharmaceutical compound for the source of magnesium ion, which is the major and essential intracellular mineral for more than 300 enzymes, DNA and RNA synthesis, reproduction and protein synthesis and also a vital coherent controller of glycolysis and the Krebs cycle in our body [1-3]. Scientific literature demonstrated that magnesium gluconate is a potent antioxidant agent and is more physiologically acceptable salt with providing highest level of magnesium among the other commercially available magnesium salts such as chloride, sulfate, citrate, lactate, aspartate, etc. [4-6]. Thus, magnesium gluconate has the wide application for magnesium supplementation in hypomagnesemia. Magnesium gluconate is used for the prevention and treatment of several diseases, such as cancer, diabetes mellitus, allergies, septic shock, inflammatory diseases, immunological disorders, asthma, arrhythmias, acute myocardial infarction, gestational hypertension, preeclampsia, eclampsia, hearing loss, oxidative stress induced ischemia/reperfusion injury, etc. [5-11]. Magnesium gluconate can be used as an oral tocolytic agent [12], neuroprotective [13], and also used in a skin-tightening cosmetic composition [14]. Subsequently, magnesium gluconate was considered as one of the components in a novel proprietary herbomineral formulation, which is designed as nutraceutical for the source of magnesium ion.

Since ancient times, many different cultures, religions, and systems of belief have recognized a living force that preserves and inhabits every living organism. This force is the source of 'life' and has been called various names, such as prana by the Hindus, *qi* or *chi* by the Chinese, and *ki* by the Japanese. This is believed to co-relate with the soul, spirit and mind. This hypothetical vital force has been scientifically evaluated and is now considered the Bioenergetics Field. The Biofield Energy is a dynamic electromagnetic field surrounding the human body, resulting from the continuous emission of low-level light, heat, and acoustical energy from the body. Biofield Energy is infinite, paradimensional and can freely flow between the human and environment [15]. Thus, a human has the ability to harness energy from the ionosphere of the earth, the "universal energy field", and transmit it to any living organism (s) or nonliving object (s) around the globe. The object or recipient always receives the energy and responds in a useful way. This process is known as The Trivedi Effect<sup>®</sup> - Biofield Energy Healing Treatment [16, 17]. Biofield (Putative Energy Field) based Energy Therapies are used worldwide to promote health and healing. The National Center of Complementary and Integrative

Health (NCCIH) has recognized and accepted Biofield Energy Healing as a Complementary and Alternative Medicine (CAM) health care approach in addition to other therapies, medicines and practices such as natural products, deep breathing, yoga, Tai Chi, Qi Gong, chiropractic/osteopathic manipulation, meditation, massage, special diets, homeopathy, progressive relaxation, guided imagery, acupressure, acupuncture, relaxation techniques, hypnotherapy, healing touch, movement therapy, pilates, rolfing structural integration, mindfulness, Ayurvedic medicine, traditional Chinese herbs and medicines, naturopathy, essential oils, aromatherapy, Reiki, cranial sacral therapy and applied prayer (as is common in all religions, like Christianity, Hinduism, Buddhism and Judaism) [18]. Biofield Energy Healing Treatment (The Trivedi Effect<sup>®</sup>) has been published in numerous peer-reviewed science journals due to its significant impacts in the science fields of biotechnology [19, 20], genetics [21, 22], cancer [23], microbiology [24-26], materials science [27, 28], agriculture [29, 30], pharmaceuticals [31, 32], nutraceuticals [33, 34], organic compounds [35, 36]. These publications reported that Biofield Energy Treatment (The Trivedi Effect<sup>®</sup>) has the significant capability to alter the physical, structural, chemical, thermal, and behavioral properties of the wide varieties of living and non-living substances. Although magnesium gluconate displayed highest bioavailability and moderate solubility in water in comparison to other magnesium salts, humans still face problems in achieving their daily requirements of magnesium [37]. The physical and chemical properties such as particle size, crystalline structure, crystallite size, surface area, etc. of a pharmaceutical have a direct influence on the absorption, dissolution, and bioavailability of the drug [38]. The stability of a solid drug with respect to the atmospheric conditions is very important to the pharmaceutical industry during processing, formulation, storage, and packaging in order to achieve better therapeutic efficacy [39]. Biofield Energy Treatment (The Trivedi Effect<sup>®</sup>) has been reported to change the particle size, specific surface area, crystalline, chemical and thermal behavior of an atom/ion through possible mediation of neutrinos [40]. Scientific literature mentions that powder X-ray diffraction (PXRD), particle size distribution analysis (PSD), Fourier transform infrared (FT-IR) spectrometry, ultraviolet-visible (UV-vis) spectroscopy, thermogravimetric analysis (TGA), and differential scanning calorimetry (DSC) analysis play an vital role for solving various problems encountered in industries for the pharmaceutical/nutraceutical formulation and developments [41]. By considering these aspects, the physicochemical, structural, thermal, and behavioral properties of the Biofield

Energy Treated and untreated magnesium gluconate were studied using various analytical techniques including PXRD, PSD, FT-IR, UV-vis spectroscopy, TGA, and DSC.

## 2. Materials and Methods

### 2.1. Chemicals and Reagents

Magnesium gluconate hydrate was procured from Tokyo Chemical Industry Co., Ltd. (TCI), Japan. All other chemicals used in the experiment were of analytical grade available in India.

### 2.2. Energy of Consciousness Healing Treatment Strategies

Magnesium gluconate was one of the components of the new proprietary herbomineral formulation, which was developed by our research team and was used *per se* as the test compound for the current study. The test compound was divided into two parts, one part of the test compound did not receive any sort of treatment and was defined as the untreated or control magnesium gluconate sample. The second part of the test compound was denoted as the Biofield Energy Treated (The Trivedi Effect<sup>®</sup> Treated) sample. Second part of the test compound was subjected to The Trivedi Effect<sup>®</sup> - Energy of Consciousness Healing Treatment (Biofield Energy Healing Treatment) by a group of twenty renowned Biofield Energy Healers remotely. Thirteen Biofield Energy Healers were remotely located in the U. S. A., five were located in Canada, and two were located in Australia, while the test compound was located in the research laboratory of GVK Biosciences Pvt. Ltd., Hyderabad, India. The Trivedi Effect<sup>®</sup> - Energy of Consciousness Healing Treatment (Biofield Energy Healing Treatment) was provided for 5. minutes through the Healer's Unique Energy Transmission process remotely to the test compound, which was kept under laboratory conditions. None of the Biofield Energy Healers in this study visited the laboratory in person, nor had any contact with the compounds. Similarly, the control compound was subjected to "sham" healer for 5. minutes, under the same laboratory conditions. The sham healer did not have any knowledge about the Biofield Energy Treatment. After that, the treated and untreated samples were kept in similar sealed conditions and characterized thoroughly by PXRD, PSD, FT-IR, UV-visible spectroscopy, TGA, and DSC analysis.

### 2.3. Characterization

#### 2.3.1. Powder X-ray Diffraction (PXRD) Analysis

The PXRD analysis was performed on PANalytical X'pert Pro powder X-ray diffractometer system. The X-ray of wavelength of 1.54056 Å was used. The data was collected in the form of a chart of the Bragg angle (2θ) vs. intensity, and a detailed table containing information on peak intensity counts, d value (Å), relative intensity (%), full width half maximum (FWHM) (θ°). From the XRD results, the crystallite size (G) was calculated using X'pert data collector and X'pert high score plus processing software. The

crystallite size (G) was calculated from the Scherrer equation [42, 43]. The method was based on the width of the diffraction patterns obtained in the X-ray reflected crystalline region. The crystallite size (G) was calculated by using the following equation 1:

$$G = k\lambda / (b\cos\theta) \quad (1)$$

Where, k is the equipment constant (0.5), λ is the X-ray wavelength (0.154 nm); b in radians is the full-width at half of the peaks and θ is the corresponding Bragg angle.

Percent change in crystallite size (G) was calculated using the following equation 2:

$$\% \text{ change in crystallite size} = \frac{|G_{\text{Treated}} - G_{\text{Control}}|}{G_{\text{Control}}} \times 100 \quad (2)$$

Where G<sub>Control</sub> and G<sub>Treated</sub> are the crystallite size of the control and Biofield Energy Treated samples, respectively.

A total of ~500.18 mg of the control and treated samples individually were used for the analysis and prepared by the back loading technique using the sample preparation kit. The sample was spread on the holder ring in sufficient quantity to fill the ring cavity. It was then pressed down using a powder press block and scrapped the powder that was in surplus using a glass slide in order to get a densely packed specimen. The bottom plate was placed onto the holder ring and clamped in position. The sample holder was then removed from the sample preparation table by turning it upside down. A smooth surface of the sample was obtained to ensure optimum results.

#### 2.3.2. Particle Size Distribution (PSD) Analysis

The average particle size and particle size distribution were analyzed using Malvern Mastersizer 2000, UK, with a detection range from 0.01 μm to 3000 μm. The sample unit was filled with dispersant medium and operated the stirrer at 2500 rpm. Alignment of the optics was done and taken the background measurement. After the background measurement, the sample was added in to the sample unit with constant monitoring of the obscuration. When the obscuration of the sample reached in between 15% and 20%, further addition of the sample stopped. When the obscuration was stable, the measurement was taken twice and the average was taken of the two measurements. The average histogram of the two measurements was recorded. The printout of the average histogram of the two measurements were documented in this study. Along with histogram, the data was presented in a table format which includes particle size (μm). Also, the values at below 10% level (d<sub>10</sub>), 50% level (d<sub>50</sub>), and 90% level (d<sub>90</sub>) were calculated from the histogram, and the calculations such as surface area (m<sup>2</sup>/g) were done by using Mastersizer 2000 software. The percent change in particle size (d) for at below 10% level (d<sub>10</sub>), 50% level (d<sub>50</sub>), and 90% level (d<sub>90</sub>) was calculated using the following equation 3:

$$\% \text{ change in particle size} = \frac{|d_{\text{Treated}} - d_{\text{Control}}|}{d_{\text{Control}}} \times 100 \quad (3)$$

Where,  $d_{\text{Control}}$  and  $d_{\text{Treated}}$  are the particle size ( $\mu\text{m}$ ) for at below 10% level ( $d_{10}$ ), 50% level ( $d_{50}$ ), and 90% level ( $d_{90}$ ) of the control and Biofield Energy Treated samples, respectively.

The percent change in surface area ( $S$ ) was calculated using the following equation 4:

$$\% \text{ change in surface area} = \frac{[S_{\text{Treated}} - S_{\text{Control}}]}{S_{\text{Control}}} \times 100 \quad (4)$$

Where,  $S_{\text{Control}}$  and  $S_{\text{Treated}}$  are the surface area of the control and treated samples, respectively.

### 2.3.3. Fourier Transform Infrared (FT-IR) Spectroscopy

FT-IR spectroscopy of the magnesium gluconate was performed using Spectrum Two (Perkin Elmer, USA) Fourier Transform Infrared Spectrometer with the frequency range of  $400\text{--}4000 \text{ cm}^{-1}$  by using the pressed KBr disk technique.

### 2.3.4. Ultraviolet-Visible Spectroscopy (UV-Vis) Analysis

The UV-Vis spectral analysis was carried out using Shimadzu UV-2450 with UV Probe, Japan. The spectrum was recorded using 1. cm quartz cell with a slit width of 1.0 nm. The wavelength range chosen for recording the spectra was 190–800 nm. The absorbance spectra (in the range of 0.2 to 0.9) and absorbance maximum ( $\lambda_{\text{max}}$ ) were recorded.

### 2.3.5. Thermal Gravimetric Analysis (TGA)

The TGA analysis was performed using TGA Q50 (TA Instruments, USA) at a heating rate of  $10^\circ\text{C}/\text{min}$  from room temperature *i.e.*  $25^\circ\text{C}$  to  $900^\circ\text{C}$  in a nitrogen atmosphere. A total of  $\sim 15 \text{ mg}$  of sample was weighed in a platinum crucible. In TGA, the weight loss for each step was recorded in grams as well as in percent loss with respect to the initial weight. Also, the onset, endset, and peak temperature for each step were recorded in TGA. In DTG, the onset, endset,

peak temperature, integral area of the peak and change in heat ( $\text{J/g}$ ) of each peak were recorded.

Percent change in weight loss ( $W$ ) was calculated using the following equation 5:

$$\% \text{ change in weight loss} = \frac{[W_{\text{Treated}} - W_{\text{Control}}]}{W_{\text{Control}}} \times 100 \quad (5)$$

Where  $W_{\text{Control}}$  and  $W_{\text{Treated}}$  are the weight loss of the control and treated samples, respectively.

### 2.3.6. Differential Scanning Calorimetry (DSC)

Analysis was performed using the DSC Q20 (TA Instruments, USA) Differential Scanning Calorimeter. A total of  $\sim 8.23 \text{ mg}$  of sample was weighed and sealed in an aluminum pan and equilibrated at  $25^\circ\text{C}$  and heated up to  $450^\circ\text{C}$  at the heating rate of  $10^\circ\text{C}/\text{min}$  under nitrogen gas as purge atmosphere with the flow rate of  $50 \text{ mL}/\text{min}$ . The value for onset, endset, peak temperature, peak height (mJ or mW), peak area, and change in heat ( $\text{J/g}$ ) for each peak were recorded.

The percent change in melting point ( $T$ ) was calculated using the following equation 6:

$$\% \text{ change in melting point} = \frac{[T_{\text{Treated}} - T_{\text{Control}}]}{T_{\text{Control}}} \times 100 \quad (6)$$

Where,  $T_{\text{Control}}$  and  $T_{\text{Treated}}$  are the melting point of the control and treated samples, respectively.

The percent change in the latent heat of fusion ( $\Delta H$ ) was calculated using the following equation 7:

$$\% \text{ change in latent heat of fusion} = \frac{[\Delta H_{\text{Treated}} - \Delta H_{\text{Control}}]}{\Delta H_{\text{Control}}} \times 100 \quad (7)$$

Where  $\Delta H_{\text{Control}}$  and  $\Delta H_{\text{Treated}}$  are the latent heat of fusion of the control and treated samples, respectively.

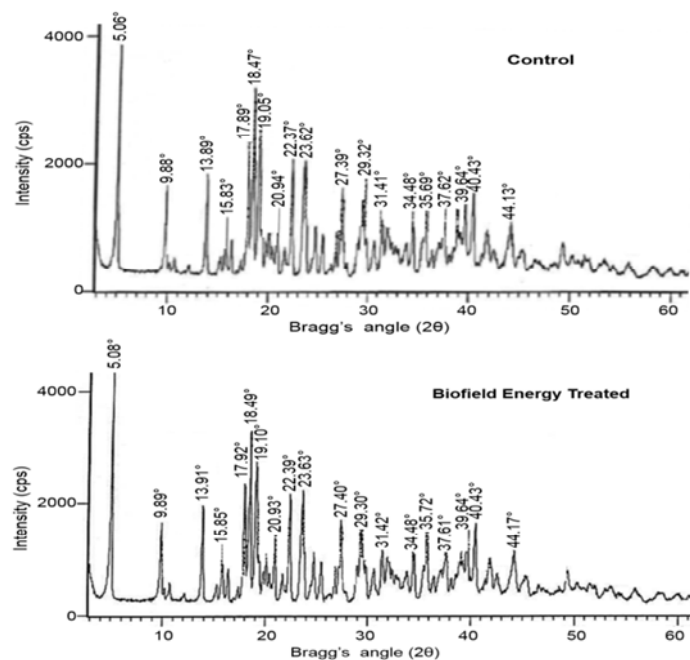


Figure 1. X-ray diffractograms of the control and Biofield Energy Treated magnesium gluconate.

Table 1. PXRD data for the control and Biofield Energy Treated magnesium gluconate.

Entry No.	Bragg angle ( $2\theta$ )		Relative Intensity (%)		FWHM ( $2\theta$ )		Crystallite size (G, nm)		% change*
	Control	Treated	Control	Treated	Control	Treated	Control	Treated	
1	5.06	5.08	100.00	100.00	0.0836	0.0836	52.70	52.70	0.00
2	9.88	9.89	39.34	32.89	0.1506	0.0836	29.34	52.85	80.14
3	13.89	13.91	43.54	40.40	0.1004	0.1506	44.17	29.44	-33.33
4	15.83	15.85	25.80	24.48	0.1004	0.1506	44.26	29.51	-33.33
5	17.89	17.92	53.13	51.40	0.1171	0.1428	38.05	31.21	-17.99
6	18.02	18.01	36.78	43.57	0.0669	0.102	66.62	43.69	-34.41
7	18.47	18.49	78.76	74.77	0.1171	0.1428	38.08	31.23	-17.99
8	19.05	19.10	66.36	57.60	0.0816	0.2244	54.70	19.89	-63.63
9	20.94	20.93	27.67	29.36	0.1338	0.1632	33.46	27.43	-18.02
10	22.37	22.39	51.02	45.82	0.1673	0.2448	26.82	18.33	-31.66
11	23.62	23.63	47.84	48.17	0.1673	0.1836	26.88	24.50	-8.88
12	27.39	27.40	36.73	33.25	0.1338	0.1632	33.86	27.76	-18.01
13	29.32	29.33	33.35	32.01	0.1506	0.1428	30.22	31.87	5.46
14	29.55	29.56	25.87	25.23	0.0669	0.0816	68.06	55.80	-18.01
15	31.41	31.42	25.06	21.94	0.1004	0.2040	45.55	22.42	-50.78
16	31.88	31.88	22.38	19.23	0.1428	0.2040	32.06	22.44	-30.00
17	34.48	34.49	23.46	21.04	0.1004	0.1428	45.91	32.28	-29.69
18	35.69	35.73	30.37	29.77	0.1840	0.1632	25.14	28.34	12.76
19	37.62	37.62	23.91	21.88	0.1506	0.2448	30.89	19.00	-38.48
20	39.64	39.65	31.87	30.95	0.0669	0.1224	69.96	38.24	-45.34
21	40.43	40.43	36.68	34.72	0.1338	0.1836	35.07	25.56	-27.12
22	44.13	44.17	24.38	22.25	0.1506	0.1224	31.55	38.82	23.06
Average crystallite size							41.06	31.97	-22.14

FWHM: Full width half maximum, \*denotes the percentage change in the crystallite size of the Trivedi Effect<sup>®</sup> Biofield Energy Treated sample with respect to the control sample.

### 3. Results and Discussion

#### 3.1. Powder X-ray Diffraction (PXRD) Analysis

The PXRD diffractograms of both the control and treated magnesium gluconate are shown in Figure 1. The diffractograms exhibited sharp and intense peaks indicating that both the samples were crystalline in nature. PXRD data such as the Bragg angle ( $2\theta$ ), relative intensity (%), full width half maximum (FWHM) ( $\theta^\circ$ ), and crystallite size (G) for the control and treated magnesium gluconate are presented in Table 1.

The crystallite size was calculated using Scherrer equation [42, 43]. The highest intense peak in both the control and treated samples was found at Bragg's angle ( $2\theta$ ) equal to  $5.06^\circ$  without any change in its crystallite size (Table 1, entry 1). Table 1. showed the significant variations of the relative intensities and crystallite size of the XRD peaks at the respective Bragg's angle ( $2\theta$ ) of both control and Biofield Energy Treated magnesium gluconate. The crystallite size values at position  $2\theta$  equal to nearly  $9.9^\circ$ ,  $29.3^\circ$ ,  $35.7^\circ$ , and  $44.2^\circ$  (Table 1, entry 2, 13, 18, and 22) were significantly increased from 5.46% to 80.14% in the treated sample compared with the control sample. Consequently, the crystallite size values of the treated sample at  $2\theta$  equal to nearly  $13.9^\circ$ ,  $15.8^\circ$ ,  $17.9^\circ$ ,  $18.0^\circ$ ,  $18.5^\circ$ ,  $19.1^\circ$ ,  $20.9^\circ$ ,  $22.4^\circ$ ,  $23.6^\circ$ ,  $27.4^\circ$ ,  $29.6^\circ$ ,  $31.4^\circ$ ,  $31.9^\circ$ ,  $34.5^\circ$ ,  $37.6^\circ$ ,  $39.6^\circ$ , and  $40.4^\circ$  (Table 1, entry 3-12, 14-17, and 19-21) were significantly decreased from 8.88% to 63.63% compared with the control sample. The average crystallite size of the treated sample was significantly

decreased by 22.14% compared to the control sample. Scientific literature reported that the changes in the XRD patterns, such as crystallite size and relative intensities, indicated the modification of the morphology of the crystal as well as the proof of polymorphic transition [44-46]. As the crystal morphology of the treated sample was altered compared with the control sample, the treated sample might be a new polymorphic form of magnesium gluconate. The crystal pattern, size and even polymorphic form of a pharmaceutical plays an important role in drug solubility, dissolution and bioavailability. It has been reported in the literature that the alteration in crystal morphology has significant impact on the *in vitro* dissolution rate, which is related with the bioavailability of orally administered pharmaceutical/nutraceutical [39]. Thus, it can be concluded that the Trivedi Effect<sup>®</sup> - Biofield Energy Healing Treatment might be a very useful method for enhancing the bioavailability of magnesium gluconate.

#### 3.2. Particle Size Distribution (PSD) Analysis

The particle size values at  $d_{10}$ ,  $d_{50}$ , and  $d_{90}$  values and surface area of both the control and treated magnesium gluconate were examined and the results are represented in Table 2. The control sample exhibited a particle size values of  $d_{10}$  (7.072  $\mu\text{m}$ ),  $d_{50}$  (41.384  $\mu\text{m}$ ), and  $d_{90}$  (189.521  $\mu\text{m}$ ). After the Biofield Energy Healing Treatment, the particle size values of magnesium gluconate were observed as 6.760  $\mu\text{m}$ , 37.812  $\mu\text{m}$ , and 197.074  $\mu\text{m}$  for  $d_{10}$ ,  $d_{50}$ , and  $d_{90}$ , respectively. Thus, the particle size values at  $d_{10}$  and  $d_{50}$  of treated magnesium gluconate were significantly decreased by 4.41% and 8.63%, respectively compared with the control sample. Consequently,

the particle size at  $d_{90}$  value was increased by 3.99% in the treated sample compared with the control sample.

**Table 2.** Particle size data ( $d_{10}$ ,  $d_{50}$ , and  $d_{90}$ ) and surface area of the control and Biofield Energy Treated magnesium gluconate.

Test Item	$d_{10}$ ( $\mu\text{m}$ )	$d_{50}$ ( $\mu\text{m}$ )	$d_{90}$ ( $\mu\text{m}$ )	Surface area ( $\text{m}^2/\text{g}$ )
Control	7.072	41.384	189.521	0.346
Biofield Energy Treated	6.760	37.812	197.074	0.365
Percent change* (%)	-4.41	-8.63	3.99	5.21

\*denotes the percentage change in the particle size data ( $d_{10}$ ,  $d_{50}$ , and  $d_{90}$ ) and surface area of the Biofield Energy Treated sample with respect to the control sample.

The surface area analysis exposed that the surface area of the treated magnesium gluconate ( $0.365 \text{ m}^2/\text{g}$ ) was significantly increased by 5.21% from the surface area of the control magnesium gluconate ( $0.346 \text{ m}^2/\text{g}$ ) as shown in Table 2.

Poorly crystallized compounds possess more surface area and higher exchange capacities than well-crystallized compounds [47]. In addition, the variation of the crystal morphology in the Biofield Energy Treated sample, which was well-supported from PXRD data, may cause to alter the surface area of the Biofield Energy Treated magnesium gluconate in comparison with the control sample. It has been well established that the particle size, shape and surface area of pharmaceutical compounds have an important impact on solubility, dissolution and *in vivo* bioavailability, as well as in helping the design of new drug delivery systems [48, 49]. Reduced particle size and higher surface area would increase the solubility of the solid particles, and consequently would improve the dissolution rate and bioavailability [50]. Thus, it is assumed that the Trivedi Effect<sup>®</sup> Biofield Energy Treated magnesium gluconate might be dissolved and absorbed at a faster rate and may possibly have more bioavailability than normal magnesium gluconate.

### 3.3. Fourier Transform Infrared (FT-IR) Spectroscopy

The FT-IR spectra of both the control and Biofield Energy Treated magnesium gluconate shown in Figure 2, exhibited only one broad band with high intensity at  $3398 \text{ cm}^{-1}$ , which was attributed to the stretching vibrations of the hydroxyl groups originating from the water present in the magnesium gluconate hydrate. The bands of stretching vibrations of primary and secondary hydroxyl groups from the gluconate part of the compound appeared in this region. These bands were remained invisible due to the intensive broad band of water [51].

The absorption peaks for the deformation vibration of the hydroxyl groups in the plane  $\delta$  (OH) and out-of-plane  $\gamma$  (OH) indicating the presence of primary and secondary hydroxyl groups, which were found at  $1434 \text{ cm}^{-1}$ ,  $636 \text{ cm}^{-1}$ , and  $583 \text{ cm}^{-1}$  in the spectrum of the control sample. However, the vibration bands for the of primary and secondary hydroxyl groups were observed in the spectra of the treated magnesium gluconate at  $1435 \text{ cm}^{-1}$ ,  $636 \text{ cm}^{-1}$ , and  $577 \text{ cm}^{-1}$ . The FT-IR spectra of the control and treated samples showed C-H stretching at  $2935 \text{ cm}^{-1}$  and  $1381 \text{ cm}^{-1}$ , respectively. A very sharp and intensive band at  $1606 \text{ cm}^{-1}$  for C=O

stretching vibration of a carbonyl group of carboxylate anion was observed in the spectra of both the control and Biofield Energy Treated samples. The band of the C-O stretching vibrations of the primary alcohol group was observed in the spectra of the control and treated samples at  $1057 \text{ cm}^{-1}$ . The absorption peaks at  $1231 \text{ cm}^{-1}$  and  $1142 \text{ cm}^{-1}$  due to the C-O stretching vibrations of the secondary alcohol groups were observed in the spectra of both the control and treated samples. The FT-IR analysis indicated that there was no significant change of the characteristic vibrational bands for the functional groups. Hence, it can be concluded that the structure of the magnesium gluconate remained the same in both the treated and control samples.

### 3.4. Ultra Violet-Visible Spectroscopy (UV-Vis) Analysis

Literature reported that 0.1% aqueous solution of magnesium gluconate showed a maximum absorption peak ( $\lambda_{\text{max}}$ ) at  $194.7 \text{ nm}$  [52]. The UV-vis spectra of both the control and treated samples (Figure 3) displayed that the wavelength for the maximum absorbance ( $\lambda_{\text{max}}$ ) of both the control and treated samples were at  $200.2 \text{ nm}$  and  $200.4 \text{ nm}$ , respectively with a minor shift of absorbance maxima from 1.8836 (control sample) to 1.8668 (Biofield Energy Treated sample).

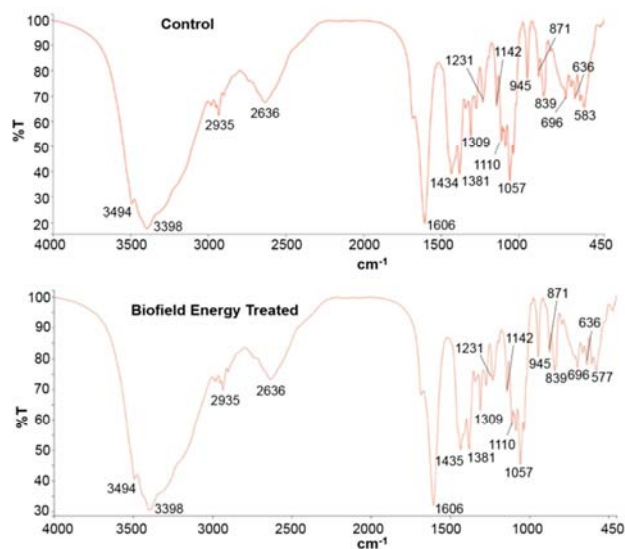


**Figure 2.** FT-IR spectra of the control and Biofield Energy Treated magnesium gluconate.

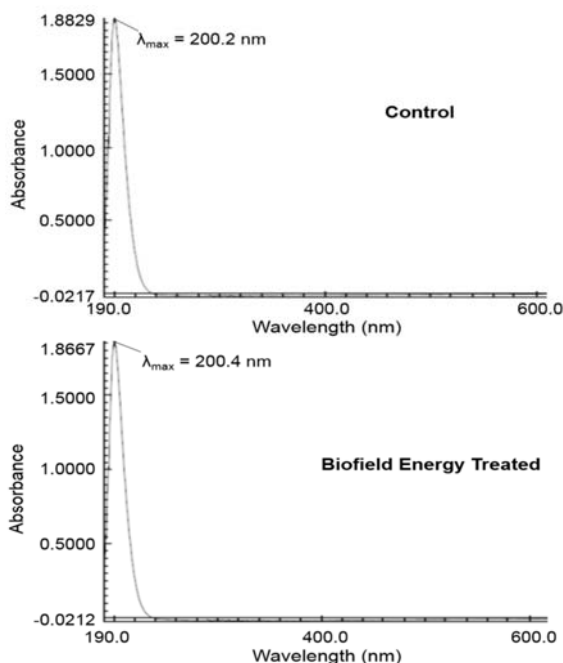


Figure 3. UV-Vis spectra of the control and Biofield Energy Treated magnesium gluconate.

The UV absorbance happens due to the different types of energy transitions from the singlet to the singlet excited state such as  $\sigma \rightarrow \sigma^*$ ,  $n \rightarrow \pi^*$ , and  $\pi \rightarrow \pi^*$ . These types of electronic transitions are happened when the difference in energy between the lowest unoccupied molecular orbital (LUMO) and the highest occupied molecular orbital (HOMO) is significantly higher than the activation energy of the compound [53]. As there was no significant change in the  $\lambda_{\max}$  of the Biofield Energy Treated sample compared with the control, it is inferred that the structural configuration or activation energy of the treated sample was not different from the control sample.

### 3.5. Thermal Gravimetric Analysis (TGA)

The TGA and DSC are very useful techniques for the evaluation of the thermal stabilities of pharmaceutical solids, determination of several kinetic parameters, and accomplishment of drug/excipient compatibility data for the pre-formulation study [54]. The TGA study of both the control and the Biofield Energy Treated magnesium gluconate (Figure 4) exhibited four thermal degradation steps and the data are presented in Table 3.

Table 3. Thermal degradation steps of the control and Biofield Energy Treated magnesium gluconate.

S. No.	Temperature (°C)		% Weight loss		% Change*
	Control	Treated	Control	Treated	
1 <sup>st</sup> step of degradation	74.86	68.65	1.12	1.09	-2.68
2 <sup>nd</sup> step of degradation	188.62	184.89	8.71	8.34	-4.25
3 <sup>rd</sup> step of degradation	300.51	300.51	38.12	38.64	1.36
4 <sup>th</sup> step of degradation	595.89	595.77	24.81	21.57	-13.06
Total weight loss	--	--	72.76	69.64	-4.29

\*denotes the percentage change in the weight loss of the Biofield Energy Treated sample with respect to the control sample.

The weight loss of the treated sample at the first, second, and fourth steps of thermal degradation were significantly reduced by 2.68%, 4.25%, and 13.06%, respectively compared with the control sample. Consequently, the weight loss of the treated magnesium gluconate at the third step of degradation was increased by 1.36% compared with the control sample. The first step degradation was probably associated with the removal of water in both the samples.

The total weight loss was 72.76% and 69.64% in the control and treated samples, respectively from their initial weight from room temperature to 600°C (Table 3). Thus, the total weight loss of the Biofield Energy Treated sample was significantly decreased by 4.29% compared with the control sample.

### 3.6. Differential Scanning Calorimetry (DSC) Analysis

The DSC thermograms of both the control and treated magnesium gluconate (Figure 5) showed two endothermic peaks. Their DSC data are presented in Table 4. The first broaden endothermic (minor) peak was due to removal the water from the sample. The second sharp endothermic (major) peak was due to the melting temperature of the magnesium gluconate.

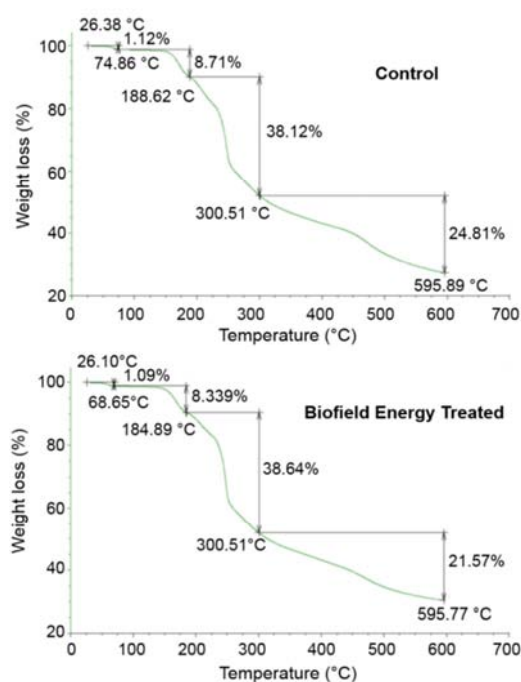


Figure 4. TGA thermograms of the control and Biofield Energy Treated magnesium gluconate.

The DSC data analysis (Table 4) revealed that the melting temperature of the treated sample (170.93°C) was almost similar with the control sample (171.02°C). But the latent

heat of fusion in the treated magnesium gluconate was significantly increased by 32.33% compared with the control sample (Table 4).

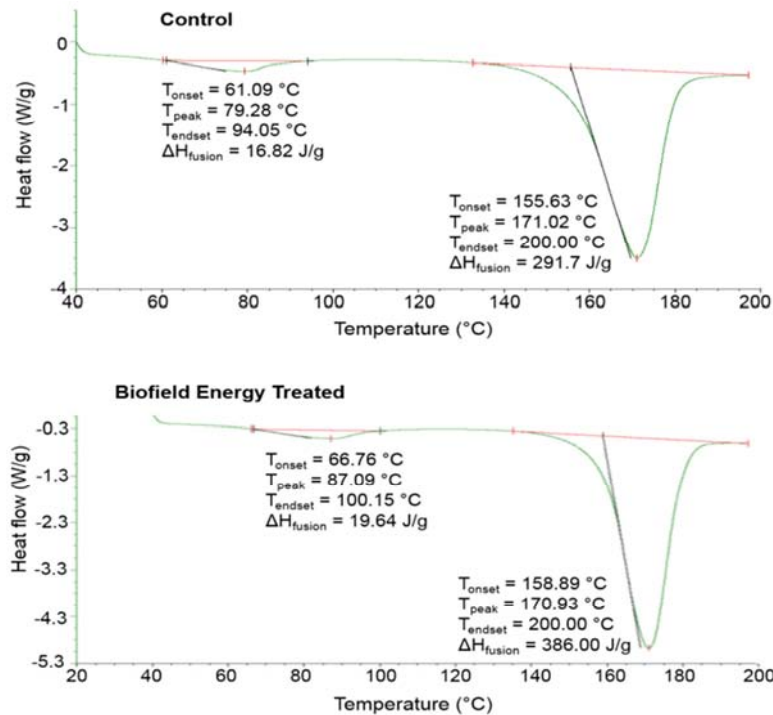


Figure 5. DSC thermograms of the control and Biofield Energy Treated magnesium gluconate.

Table 4. The latent heat of fusion (J/G) and melting point (°C) values of the control and Biofield Energy Treated magnesium gluconate.

Endothermic peak	Description	T <sub>onset</sub> (°C)	T <sub>peak</sub> (°C)	T <sub>endset</sub> (°C)	ΔH <sub>fusion</sub> (J/g)
Minor peak	Control sample	61.09	79.28	94.05	16.82
	Biofield Treated sample	66.76	87.09	100.15	19.64
	% Change*	9.28	9.85	6.49	16.77
Major peak	Control sample	155.63	171.02	200.00	291.70
	Biofield Treated sample	158.89	170.93	200.00	386.00
	% Change*	2.09	-0.05	0.00	32.33

T<sub>onset</sub>: Onset melting temperature, T<sub>peak</sub>: Peak melting temperature, T<sub>endset</sub>: Endset melting temperature, ΔH: Latent heat of fusion, \*denotes the percentage change of Biofield Energy Treated sample with respect to the control sample.

Additionally, the temperature for water removal and the latent heat of fusion from the treated sample was significantly increased by 9.85% and 16.77%, respectively compared with the control sample. The analysis indicated that the thermal stability of the treated sample was significantly improved compared with the control sample.

### 4. Conclusions

The current analysis anticipated the significant effect of The Trivedi Effect<sup>®</sup> - Energy of Consciousness Healing Treatment (Biofield Energy Healing Treatment) on physicochemical, thermal and behavioral properties of magnesium gluconate. The PXRD analysis showed that the crystallite size was significantly transformed from -63.63% to 80.14% in the treated magnesium gluconate compared with the control sample. The average crystallite size of the treated sample was significantly decreased by 22.14% compared with the control sample. Overall, the PXRD

analysis exposed that the crystal morphology of the treated sample was significantly altered compared with the control sample. PSD analysis revealed that the particle size values at d<sub>10</sub> and d<sub>50</sub> values were significantly decreased by 4.41%, and 8.67%, respectively in the treated sample compared with the control sample. Whereas, the particle size at d<sub>90</sub> value in the treated sample was enhanced by 3.99% compared to the control sample. The surface area analysis revealed that surface area of the treated sample was significantly increased by 5.21% compared with the control sample. The TGA analysis showed four steps thermal degradation of both the samples and the total weight loss was reduced by 4.29% in the treated sample compared with the control sample. The DSC analysis demonstrated that the melting temperature of the treated sample (170.93°C) was almost identical with the control sample (171.02°C). The latent heat of fusion of the treated sample was significantly increased by 32.33% compared to the control sample. The TGA and DSC analysis clearly indicated that the thermal stability of the treated



sample was significantly enhanced compared with the control sample. Thus, The Trivedi Effect<sup>®</sup> Treated magnesium gluconate would be a new polymorphic form of magnesium gluconate, which could be more soluble and bioavailable along with improved thermal stability compared with the untreated magnesium gluconate. Briefly, The Trivedi Effect<sup>®</sup> - Energy of Consciousness Healing Treatment (Biofield Energy Healing Treatment) could be a useful approach in the design of better nutraceutical and/or pharmaceutical formulations that can offer significant therapeutic responses against various diseases such as diabetes mellitus, allergies and septic shock; stress-related disorders like sleep disorder, insomnia, anxiety, depression, Attention Deficit Disorder (ADD), Attention Deficit Hyperactive Disorder (ADHD), mental restlessness (mind chattering), brain fog, low libido, impotency, lack of motivation, mood swings, fear of the future, confusion, migraines, headaches, forgetfulness, overwhelm, loneliness, worthlessness, indecisiveness, frustration, irritability, chronic fatigue, obsessive/compulsive behavior and panic attacks; inflammatory diseases and immunological disorders like Lupus, Systemic Lupus Erythematosus, Hashimoto Thyroiditis, Type 1. Diabetes, Asthma, Chronic peptic ulcers, Tuberculosis, Hepatitis, Chronic active hepatitis, Celiac Disease (gluten-sensitive enteropathy), Addison Disease, Crohn's disease, Graves' Disease, Pernicious and Aplastic Anemia, Sjogren Syndrome, Irritable Bowel Syndrome (IBS), Multiple Sclerosis, Rheumatoid arthritis, Chronic periodontitis, Ulcerative colitis, Chronic sinusitis, Myasthenia Gravis, Atherosclerosis, Vasculitis, Dermatitis, Diverticulitis, Rheumatoid Arthritis, Reactive Arthritis, Alopecia Areata, Psoriasis, Scleroderma, Fibromyalgia, Chronic Fatigue Syndrome and Vitiligo; aging-related diseases like cardiovascular disease, arthritis, cancer, Alzheimer's disease, dementia, cataracts, osteoporosis, diabetes, hypertension, glaucoma, hearing loss, Parkinson's Disease, Huntington's Disease, Prion Disease, Motor Neurone Disease, Spinocerebellar Ataxia, Spinal muscular atrophy, Amyotrophic lateral sclerosis, Friedreich's Ataxia and Lewy Body Disease; chronic infections and many more.

## Abbreviations

DSC: Differential scanning calorimetry, FT-IR: Fourier transform infrared spectroscopy, FWHM: Full width half maximum, G: Crystallite size, HOMO: Highest energy occupied molecular orbital, LUMO: Lowest energy unoccupied molecular orbital, TGA: Thermal gravimetric analysis,  $T_{\text{onset}}$ : Onset melting temperature,  $T_{\text{peak}}$ : Peak melting temperature,  $T_{\text{endset}}$ : Endset melting temperature,  $\Delta H$ : Latent heat of fusion, UV-vis: Ultraviolet-visible spectroscopy, PSD: Particle size distribution; PXRD: Powder X-ray diffraction.

## Acknowledgements

The authors are grateful to GVK Biosciences Pvt. Ltd.,

Trivedi Science, Trivedi Global, Inc., and Trivedi Master Wellness for their assistance and support during this work.

## References

- [1] Heaton FW (1990) Role of magnesium in enzyme systems in metal ions in biological systems, In: Sigel H, Sigel A (Eds.), Volume 26. Compendium on magnesium and its role in biology, nutrition and physiology, Marcel Dekker Inc., New York.
- [2] Frick DN, Banik S, Rypma RS (2007) Role of divalent metal cations in ATP hydrolysis catalyzed by the hepatitis C virus NS3 helicase: Magnesium provides a bridge for ATP to fuel unwinding. *J Mol Biol* 365: 1017-1032.
- [3] Garfinkel L, Garfinkel D (1985) Magnesium regulation of the glycolytic pathway and the enzymes involved. *Magnesium* 4: 60-72.
- [4] Coudray C, Rambeau M, Feillet-Coudray C, Gueux E, Tressol JC, Mazur A, Rayssiguier Y (2005) Study of magnesium bioavailability from ten organic and inorganic Mg salts in Mg-depleted rats using a stable isotope approach. *Magn Res* 18: 215-223.
- [5] Fleming TE, Mansmann Jr HC (1999) Methods and compositions for the prevention and treatment of diabetes mellitus. United States Patent 5871769, 1-10.
- [6] Fleming TE, Mansmann Jr HC (1999) Methods and compositions for the prevention and treatment of immunological disorders, inflammatory diseases and infections. United States Patent 5939394, 1-11.
- [7] Guerrero MP, Volpe SL, Mao JJ (2009) Therapeutic uses of magnesium. *Am Fam Physician* 80: 157-162.
- [8] Gums JG (2004) Magnesium in cardiovascular and other disorders. *Am J Health Syst Pharm* 61: 1569-1576.
- [9] Gröber U, Schmidt J, Kisters K (2015) Magnesium in prevention and therapy. *Nutrients* 7: 8199-8226.
- [10] Clague JE, Edwards RH, Jackson MJ (1992) Intravenous magnesium loading in chronic fatigue syndrome. *Lancet* 340: 124-125.
- [11] Weglicki WB (2000) Intravenous magnesium gluconate for treatment of conditions caused by excessive oxidative stress due to free radical distribution. United States Patent 6100297, 1-6.
- [12] Martin RW, Martin JN Jr, Pryor JA, Gaddy DK, Wiser WL, Morrison JC (1988) Comparison of oral ritodrine and magnesium gluconate for ambulatory tocolysis. *Am J Obstet Gynecol* 158: 1440-1445.
- [13] Turner RJ, Dasilva KW, O'Connor C, van den Heuvel C, Vink R (2004) Magnesium gluconate offers no more protection than magnesium sulphate following diffuse traumatic brain injury in rats. *J Am Coll Nutr* 23: 541S-544S.
- [14] Lee KH, Chung SH, Song JH, Yoon JS, Lee J, Jung MJ, Kim JH (2013) Cosmetic compositions for skin-tightening and method of skin-tightening using the same. United States Patent 8580741 B2.

- [15] Stenger VJ (1999) Bioenergetic fields. *Sci Rev Alternative Med* 3.
- [16] Warber SL, Cornelio D, Straughn J, Kile G (2004) Biofield energy healing from the inside. *J Altern Complement Med* 10: 1107-1113.
- [17] Rubik B (2002) The biofield hypothesis: Its biophysical basis and role in medicine. *J Altern Complement Med* 8: 703-717.
- [18] Koithan M (2009) Introducing complementary and alternative therapies. *J Nurse Pract* 5: 18-20.
- [19] Trivedi MK, Branton A, Trivedi D, Nayak G, Bairwa K, Jana S (2015) Characterization of physicochemical and spectroscopic properties of biofield energy treated biopeptone. *Advances in Bioscience and Bioengineering* 3: 59-66.
- [20] Trivedi MK, Branton A, Trivedi D, Nayak G, Bairwa K, Jana S (2015) Physicochemical and spectroscopic characterization of yeast extract powder after the biofield energy treatment. *American Journal of Life Sciences* 3: 387-394.
- [21] Trivedi MK, Branton A, Trivedi D, Nayak G, Gangwar M, Jana S (2015) Antibiofilm, biochemical reactions, and genotypic pattern of biofield treated *Pseudomonas aeruginosa*. *J Trop Dis* 4: 181
- [22] Trivedi MK, Branton A, Trivedi D, Nayak G, Mondal SC, Jana S (2015) Evaluation of antibiogram, genotype and phylogenetic analysis of biofield treated *Nocardia otitidis*. *Biol Syst Open Access* 4: 143.
- [23] Trivedi MK, Patil S, Shettigar H, Mondal SC, Jana S (2015) The potential impact of biofield treatment on human brain tumor cells: A time-lapse video microscopy. *J Integr Oncol* 4: 141.
- [24] Trivedi MK, Patil S, Shettigar H, Mondal SC, Jana S (2015) Antimicrobial susceptibility pattern and biochemical characteristics of *Staphylococcus aureus*: Impact of biofield treatment. *J Microb Biochem Technol* 7: 238-241.
- [25] Trivedi MK, Patil S, Harish S, Gangwar M, Jana S (2015) Biofield Treatment: An alternative approach to combat multidrug-resistant susceptibility pattern of *Raoultella ornithinolytica*. *Altern Integr Med* 4: 193.
- [26] Trivedi MK, Branton A, Trivedi D, Nayak G, Mondal SC, Jana S (2015) *In vitro* evaluation of biofield treatment on viral load against human immunodeficiency-1 and cytomegaloviruses. *American Journal of Health Research* 3: 338-343.
- [27] Trivedi MK, Tallapragada RM, Branton A, Trivedi D, Nayak G, Latiyal O, Jana S (2015) Characterization of physical, thermal and structural properties of chromium (VI) oxide powder: Impact of biofield treatment. *J Powder Metall Min* 4: 128.
- [28] Trivedi MK, Tallapragada RM, Branton A, Trivedi D, Nayak G, Latiyal O, Jana S (2015) Potential impact of biofield energy treatment on the atomic, physical and thermal properties indium powder. *J Material Sci Eng* 4: 198.
- [29] Trivedi MK, Branton A, Trivedi D, Nayak G, Mondal SC, Jana S (2015) Impact of biofield energy treatment on soil fertility. *Earth Sciences* 4: 275-279.
- [30] Trivedi MK, Branton A, Trivedi D, Nayak G, Gangwar M, Jana S (2015) Agronomic characteristics, growth analysis, and yield response of biofield treated mustard, cowpea, horse gram, and groundnuts. *International Journal of Genetics and Genomics* 3: 74-80.
- [31] Trivedi MK, Patil S, Shettigar H, Bairwa K, Jana S (2015) Spectroscopic characterization of chloramphenicol and tetracycline: An impact of biofield. *Pharm Anal Acta* 6: 395.
- [32] Trivedi MK, Patil S, Shettigar H, Bairwa K, Jana S (2015) Spectroscopic characterization of biofield treated metronidazole and tinidazole. *Med chem* 5: 340-344.
- [33] Trivedi MK, Tallapragada RM, Branton A, Trivedi D, Nayak G, Latiyal O, Jana S (2015) Physical, atomic and thermal properties of biofield treated lithium powder. *J Adv Chem Eng* 5: 136.
- [34] Trivedi MK, Tallapragada RM, Branton A, Trivedi D, Nayak G, Mishra RK, Jana S (2015) Biofield treatment: A potential strategy for modification of physical and thermal properties of gluten hydrolysate and ipomoea macroelements. *J Nutr Food Sci* 5: 414.
- [35] Trivedi MK, Branton A, Trivedi D, Nayak G, Bairwa K, Jana S (2015) Physicochemical and spectroscopic characterization of *p*-chlorobenzaldehyde: an impact of biofield energy treatment. *Insights in Analytical Electrochemistry* 1: 5.
- [36] Trivedi MK, Branton A, Trivedi D, Nayak G, Latiyal O, Jana S (2015) Evaluation of biofield treatment on atomic and thermal properties of ethanol. *Organic Chem Curr Res* 4: 145.
- [37] Ranade VV, Somberg JC (2001) Bioavailability and pharmacokinetics of magnesium after administration of magnesium salts to humans. *Am J Ther* 8: 345-357.
- [38] Chereson R (2009) Bioavailability, bioequivalence, and drug selection. In: Makoid CM, Vuchetich PJ, Banakar UV (eds) *Basic pharmacokinetics (1<sup>st</sup> Edn)* Pharmaceutical Press, London.
- [39] Blagden N, de Matas M, Gavan PT, York P (2007) Crystal engineering of active pharmaceutical ingredients to improve solubility and dissolution rates. *Adv Drug Deliv Rev* 59: 617-630.
- [40] Trivedi MK, Mohan TRR (2016) Biofield energy signals, energy transmission and neutrinos. *American Journal of Modern Physics* 5: 172-176.
- [41] Chauhan A, Chauhan P (2014) Powder XRD technique and its applications in science and technology. *J Anal Bioanal Tech* 5: 212.
- [42] Alexander L, Klug HP (1950) Determination of crystallite size with the X-Ray spectrometer. *J App Phys* 21: 137.
- [43] Langford JI, Wilson AJC (1978) Scherrer after sixty years: A survey and some new results in the determination of crystallite size. *J Appl Cryst* 11: 102-113.
- [44] Inoue M, Hirasawa I (2013) The relationship between crystal morphology and XRD peak intensity on CaSO<sub>4</sub>·2H<sub>2</sub>O. *J Crystal Growth* 380: 169-175.
- [45] Raza K, Kumar P, Ratan S, Malik R, Arora S (2014) Polymorphism: The phenomenon affecting the performance of drugs. *SOJ Pharm Pharm Sci* 1: 10.
- [46] Brittain HG (2009) Polymorphism in pharmaceutical solids in *Drugs and Pharmaceutical Sciences*, volume 192, 2<sup>nd</sup> Edn, Informa Healthcare USA, Inc., New York.

- [47] Murray HH, Lyons SC (1960) Further correlation of kaolinite crystallinity with chemical and physical properties. *Clays Clay Miner* 8: 11-17.
- [48] Sun J, Wang F, Sui Y, She Z, Zhai W, Wang C, Deng Y (2012) Effect of particle size on solubility, dissolution rate, and oral bioavailability: Evaluation using coenzyme Q<sub>10</sub> as naked nanocrystals. *Int J Nanomed* 7: 5733-5744.
- [49] Khadka P, Ro J, Kim H, Kim I, Kim JT, Kim H, Cho JM, Yun G, Lee J (2014) Pharmaceutical particle technologies: An approach to improve drug solubility, dissolution and bioavailability. *Asian J Pharm Sci* 9: 304-316.
- [50] Buckton G, Beezer AE (1992) The relationship between particle size and solubility. *Int J Pharmaceutics* 82: R7-R10.
- [51] Nikolic VD, Illic DP, Nikolic LB, Stanojevic LP, Cakic MD, Tacic AD, Ilic-Stojanovic SS (2014) The synthesis and characterization of iron (II) gluconate. *Advanced Technologies* 3: 16-24.
- [52] Ji L, Yin W, Fu-Jia M (2004) Confirmation of the chemical structure of magnesium gluconate. *Pharmaceutical Care and Research* 4: 272-273.
- [53] Hesse M, Meier H, Zeeh B (1997) *Spectroscopic methods in organic chemistry*, Georg Thieme Verlag Stuttgart, New York.
- [54] Alves R, Reis TVS, Silva LCC, Storpirtis S, Mercuri LP, Matos JR (2010) Thermal behavior and decomposition kinetics of rifampicin polymorphs under isothermal and non-isothermal conditions. *Braz J Pharm Sci* 46: 343-351.